Nonadiabatic Nuclear Dynamics after Valence Ionization of H2O

3 AUTHORS, INCLUDING:

Matthis Eroms
Universität Heidelberg
5 PUBLICATIONS **30** CITATIONS

SEE PROFILE

Hans-Dieter Meyer
Universität Heidelberg
245 PUBLICATIONS **9,841** CITATIONS

SEE PROFILE

Nonadiabatic Nuclear Dynamics after Valence Ionization of H₂O[†]

Matthis Eroms,*,‡ Martin Jungen,*,§ and Hans-Dieter Meyer*,‡

Theoretische Chemie, Physikalisch-Chemisches Institut, Universität Heidelberg, INF 229, D-69120 Heidelberg, Germany, Institut für Physikalische Chemie, Universität Basel, Klingelbergstrasse 80, CH-4056 Basel, Switzerland

The gas-phase photoelectron spectrum of water in the 12−20 eV energy range is simulated. The potential energy surfaces (PESs) of the three cationic states involved show several degeneracies. The ground state (X^2B_1) and the first excited state (A^2A_1) are degenerate components of a $^2\Pi_u$ state in linear geometry leading to Renner−Teller coupling while the PESs of the A state and the second excited state (B^2B_2) exhibit a conical intersection. Thus, an adiabatic approach that relies on sufficiently separated surfaces deems inappropriate. However, an orthogonal transformation of the electronic states removes the diverging matrix elements in the kinetic energy. These diabatic states permit a correct treatment of the nuclear dynamics near a conical intersection as well as in the Renner−Teller zone. The quantum mechanical equations of motion of the nuclei are solved using the multiconfiguration time-dependent Hartree (MCTDH) method. Quantum chemical calculations for the cationic states had been performed before, using a multireference configuration interaction method.

I. Introduction

In this article the photoionization of water molecules is investigated. As in several experimental studies,[1−7] the binding energy of the photoelectrons is restrained to values between 12 and 20 eV. In this range, only electrons from the three outer valence orbitals contribute to the spectrum. The ground state electronic configuration of water is $(1a_1)^2(2a_1)^2(1b_2)^2(3a_1)^2(1b_1)^2$ (X^1A_1). Removal of one electron from the $1b_1$, $3a_1$, or $1b_2$ orbitals leads to the three "principal" Koopmans' states, X^2B_1, A^2A_1, and B^2B_2. An examination of their potential energy surfaces (PESs)[8] reveals a conical intersection between the A and B states and a Renner−Teller coupling of the X and A states as they are degenerate components of a $^2\Pi_u$ state at linear geometry. Experimental[1−3,5−7] as well as theoretical work[9−13] on the principal states of the water cation has long since dealt with these degeneracies. In an adiabatic calculation of the photoelectron spectrum, the nuclear dynamics of the molecule in its various cationic states takes place on independent PESs. As long as they are energetically well separated, this is a suitable and powerful concept, known as the Born−Oppenheimer approximation (BOA). Here, however, the energetical distances of the PESs become closer than typical vibrational excitations, which are of the order of 100 meV. Then, the derivative, or vibronic, coupling terms of the kinetic energy matrix diverge leading to a breakdown of the BOA. Hence, the electronic states cannot be regarded as independent any more.

At least for a strict two-state system, a diagonalization of the kinetic energy matrix is possible. An orthogonal transformation of the original, adiabatic, electronic states to a diabatic electronic basis permits removal of the diverging terms in the kinetic energy. Instead of the derivative coupling terms, now off-diagonal elements emerge in the potential energy. A particularly convenient way to remove at least the singular part of the vibronic coupling lies in the notion of so-called "regularized diabatic states",[14−16] which were introduced before to treat systems of two coupled states, such as the H₂S and O₃ molecules in ref 15. The main advantage is that all the necessary information is already contained in the adiabatic ab initio PESs; no further quantum chemical evaluation of coupling terms is required. A similar scheme is used here for the diabatization of the A and B electronic states.

To deal with the Renner−Teller coupled states (X and A), an approach related to a study of CO_2[17] is employed. More recently, Renner−Teller coupling was also addressed, for example, in ref 18, where the dissociative electron attachment to H₂O is discussed, and in ref 19, concerning OHF⁻. Again, no further quantum chemical calculations are needed to diagonalize the kinetic energy.

The resulting equations of motion now involve three coupled states. For the present study, wavepacket propagations as well as a calculation of vibronic eigenenergies and eigenfunctions have been performed employing the MCTDH method[20,21] to solve the time-dependent and time-independent Schrödinger equations.

This work is by no means the first theoretical study of the principal cationic states of water. Here, however, starting from ab initio PESs, the spectrum is obtained quantum mechanically and in a fully dynamic way. A time-dependent treatment of the equations of motion not only allows for a more efficient solution, it also makes a study of wavepacket dynamics feasible.

The article is organized as follows. In Section II, the equations of motions are derived. This is accompanied by a brief introduction to the concept of regularized diabatic states and the Renner−Teller Hamiltonian. Section III deals with the computational methods, and Section IV presents the results from the calculations and a comparison to the experiment.

II. Theoretical Background

In a photoelectron spectroscopy experiment, a gas sample is probed by a monochromatic photon beam. The emitted electrons

are collected by an energy analyzer. As a result, the intensity of emitted electrons versus their binding energy can be inferred since both the kinetic energy of the electrons and the excitation frequency of the light source are known. In a schematic view, an electron is removed from its orbital and is excited into the continuum, leaving the parent molecule in a singly ionized state. The electronic configuration of the ion differs from the neutral approximately only in the occupation of one molecular orbital (MO). Varying the photon energy in the experiment allows one to choose which MO will be ionized. Since the MOs contribute differently to the chemical bonding of the molecule, the equilibrium position of the nuclei in the ion will in general differ from the neutral ground state, leading to an excitation of vibrations in the molecule. The degree of vibrational excitation can be detected in the experiment if the resolution of the photoelectron spectrum is fine enough.

The ionization potentials of the three outer valence orbitals $1b_1$, $3a_1$, and $1b_2$ are between 12 and 18 eV, which is the energy range relevant for the present study as well as for several experimental works. The character of the outermost $1b_1$ orbital is essentially nonbonding.[2] It can be expected that vibrational excitation in the X state will be weak, as the geometry change is rather small. In the A band, however, the bending mode should be excited considerably, since the ion assumes a linear configuration. For the B state one can predict a mixture of both stretching and bending modes. Cuts through the surfaces are displayed in ref 8.

Theoretical considerations are facilitated if the Born−Oppenheimer approximation is valid. Here, however, the PESs of the electronic states are often closer than typical vibrational energies; at certain geometries they even touch or intersect. The resulting vibronic coupling has considerable influence on the spectrum. This has to be taken into account in a simulation of the photoelectron spectrum of water. Therefore, the Hamiltonian of the coupled three-state system has to be set up.

First, PESs of the X, A, and B state have to be obtained. This was already done for a study of the resonant Auger decay in the water molecule[8] where ab initio surfaces were evaluated for an adiabatic approach to the dynamics. These states belong to the A′ and A″ representations of the C_s symmetry group. To be precise, they are the X^2A'', A^2A', and B^2A' states, respectively. The pertaining PESs V_X, V_A, and V_B are energetically ordered. Thus, the (diagonal) adiabatic potential energy matrix **V** is

$$\mathbf{V} = \begin{pmatrix} V_X & 0 & 0 \\ 0 & V_A & 0 \\ 0 & 0 & V_B \end{pmatrix} \quad (1)$$

As was already pointed out in the Introduction, an orthogonal basis transformation **S** suppresses the singular coupling terms, on the expense of an additional potential coupling in the diabatic potential energy matrix $\mathbf{W} = \mathbf{SVS}^\dagger$. Here, this goal is reached in two steps. First, diabatic electronic states are obtained for the conically intersecting A and B states. In this step, a two-state system is assumed; the X state is excluded from transformation. Hence, the diabatic potential energy matrix $\mathbf{W}_{A,B}$ of the subsystem assumes

$$\mathbf{W}_{A,B} = \begin{pmatrix} W_{11} & W_{12} \\ W_{12} & W_{22} \end{pmatrix} \quad (2)$$

The transformation yields three matrix elements, the diabatic surfaces W_{11} and W_{22}, and a coupling term, W_{12}. By inspection of the diabatic surfaces from step one it is found that close to linearity of the molecule, W_{11} correlates with V_A and W_{22} with V_B. Further details can be found in the Appendix A.

In the second step, the Renner−Teller-coupling of the X and A states is addressed. To understand the origin of this coupling better, the kinetic energy operator **T** of the nuclei is given. In the body-fixed (BF) frame using valence coordinates (where r_1 and r_2 denote the two OH-distances and θ is the bond angle) one finds, according to ref 22

$$\mathbf{T} = \frac{\hat{p}_1^2}{2\mu_1} + \frac{\hat{p}_2^2}{2\mu_2} + \frac{\hat{j}^2}{2\mu_1 r_1^2} + \frac{\hat{j}^2}{2\mu_2 r_2^2} + \frac{\hat{p}_1 \hat{p}_2 \cos\theta}{m_O} -$$

$$\frac{\hat{p}_1 \hat{p}_\theta}{m_O r_2} - \frac{\hat{p}_2 \hat{p}_\theta}{m_O r_1} - \frac{\cos\theta \hat{j}^2 + \hat{j}^2 \cos\theta}{2 m_O r_1 r_2} + \frac{\hat{J}^2 - 2\hat{J}_z^2}{2\mu_2 r_2^2} +$$

$$\hat{J}_y \frac{\sin\theta}{m_O r_2} \hat{p}_1 - \frac{\sin\theta}{2 m_O r_1 r_2} (\hat{J}_x \hat{J}_z + \hat{J}_z \hat{J}_x) - \frac{1}{2\mu_2 r_2^2} (\hat{J}_+ \hat{j}_- +$$

$$\hat{J}_- \hat{j}_+) + \frac{1}{4 m_O r_1 r_2} (\cos\theta \hat{J}_+ \hat{j}_- + \hat{J}_+ \hat{j}_- \cos\theta + \cos\theta \hat{J}_- \hat{j}_+ +$$

$$\hat{J}_- \hat{j}_+ \cos\theta) \quad (3)$$

with the reduced masses $\mu_1 = \mu_2 = (m_O m_H)/(m_O + m_H)$.

The momentum operators are defined as

$$\hat{p}_{1,2} = -i \frac{\partial}{\partial r_{1,2}}, \quad \hat{p}_\theta = -i \frac{\partial}{\partial\theta} \sin\theta \quad (4)$$

$$\hat{j}^2 = -\frac{1}{\sin\theta} \frac{\partial}{\partial\theta} \sin\theta \frac{\partial}{\partial\theta} - \frac{1}{\sin^2\theta} \frac{\partial^2}{\partial\phi^2} \quad (5)$$

$$\hat{j}_\pm = e^{\pm i\phi} \left(\pm \frac{\partial}{\partial\theta} + i \cot\theta \frac{\partial}{\partial\phi} \right) \quad (6)$$

where ϕ denotes the azimuthal angle for rotations around the BF z-axis, which in this case is parallel to the $\vec{r}_2$ vector. The vector operator of total angular momentum is $\hat{J} = (\hat{J}_x, \hat{J}_y, \hat{J}_z)^T$ with components given in the BF frame, and, as usual, $\hat{J}_\pm = \hat{J}_x \pm i\hat{J}_y$. The explicit form of the total angular momentum operators is discussed in refs 22 and 23 but is of no further interest here.

As a next step we move from a coordinate representation of the azimuthal angle ϕ to a momentum representation. This replaces the differential operator $-i\partial/\partial\phi$ by the product operator k, for example,

$$\hat{j}^2 = -\frac{1}{\sin\theta} \frac{\partial}{\partial\theta} \sin\theta \frac{\partial}{\partial\theta} + \frac{k^2}{\sin^2\theta} \quad (7)$$

As we work in a BF frame, k is the projection of the total nuclear angular momentum on the BF z-axis.

The operators $\hat{j}_\pm$ accomplish now a shift $k \rightarrow k \pm 1$ due to the factor $e^{\pm i\phi}$. These shifts in k, which originate from the Coriolis coupling, prohibit that k becomes a good quantum number.

The centrifugal sudden approximation (also called coupled states approximation), which we will adopt next, ignores the Coriolis coupling terms and hence makes k a good quantum

number. We go a step further and also ignore the centrifugal term $(\hat{J}^2 - 2\hat{J}_z^2)/2\mu_2 r_2^2$, as in our applications we assume the total angular momentum to be small.

Hence the kinetic energy operator that we use consists only of the first eight terms of eq 3 and is thus identical to the one for $J = 0$, except that the $\hat{j}^2$ operator contains a k^2 term (see eq 7).

The Renner−Teller effect is introduced by assuming that the projection of the total angular momentum on the BF z-axis, $\hat{J}_z$, is conserved, but not the corresponding nuclear angular momentum, because the electronic angular momentum may change.

From angular momentum conservation follows

$$k = \hat{j}_z = \hat{J}_z - \hat{l}_z = K - \hat{l}_z \qquad (8)$$

where $\hat{l}_z$ is the electronic angular momentum operator and K the eigenvalue of $\hat{J}_z$. As K is a good quantum number we are allowed to replace the operator $\hat{J}_z$ by its eigenvalue.

In general, the electronic states ψ_X and ψ_A mix upon application of $\hat{l}_z$. In linear geometry, they are degenerate components of a $^2\Pi_u$ state and $\hat{l}_z\psi_{A/X} = \pm i\psi_{X/A}$. The linear combinations $\psi_\pm = (1/\sqrt{2})(\psi_A \pm i\psi_X)$, however, are eigenstates of $\hat{l}_z$ with eigenvalues ± 1. It is common to assume that this holds also for the nonlinear case as the coupling is large only at linearity of the molecule as is outlined in refs 18 and 24. Using the states $\psi_\pm$ one may replace the operator $\hat{l}_z$ by its eigenvalues, and the only modification to the kinetic energy operator is that k^2 in eq 7 is to be replaced by $(K \mp 1)^2$ for $\psi_\pm$, respectively.

The transformation to the states $\psi_\pm$ is accomplished by the matrix

$$\mathbf{S}_2 = \frac{1}{\sqrt{2}}\begin{pmatrix} i & 1 \\ -i & 1 \end{pmatrix} \qquad (9)$$

and applying this transformation to the Renner−Teller submatrix $\mathbf{V}_{X,A}$ yields

$$\mathbf{W}_{X,A} = \mathbf{S}_2\begin{pmatrix} V_X & 0 \\ 0 & V_A \end{pmatrix}\mathbf{S}_2^\dagger = \frac{1}{2}\begin{pmatrix} V_X + V_A & V_A - V_X \\ V_A - V_X & V_X + V_A \end{pmatrix} \qquad (10)$$

Note that the kinetic energy operator for the first electronic state (ψ_+) is characterized by $k = K - 1$ and the second (ψ_-) by $k = K + 1$.

Finally, we replace the adiabatic surface V_A by the diabatic one, W_{11}. It is convenient to assign the value K to the nuclear angular momentum projection when considering the diabatic state W_{22}, which correlates with V_B for large θ.

We hence introduce the transformation matrix

$$\mathbf{S}_3 = \frac{1}{\sqrt{2}}\begin{pmatrix} i & 1 & 0 \\ 0 & 0 & \sqrt{2} \\ -i & 1 & 0 \end{pmatrix} \qquad (11)$$

and the final diabatic potential matrix

$$\mathbf{W} = \mathbf{S}_3\begin{pmatrix} V_X & 0 & 0 \\ 0 & W_{11} & W_{12} \\ 0 & W_{12} & W_{22} \end{pmatrix}\mathbf{S}_3^\dagger =$$

$$\begin{pmatrix} \dfrac{W_{11} + X}{2} & \dfrac{W_{12}}{\sqrt{2}} & \dfrac{W_{11} - X}{2} \\[2mm] \dfrac{W_{12}}{\sqrt{2}} & W_{22} & \dfrac{W_{12}}{\sqrt{2}} \\[2mm] \dfrac{W_{11} - X}{2} & \dfrac{W_{12}}{\sqrt{2}} & \dfrac{W_{11} + X}{2} \end{pmatrix} \qquad (12)$$

Again, the kinetic energy operator is diagonal in the states but state dependent. It is specified by the nuclear angular momentum projection k which takes the values $K - 1$, K, $K + 1$ for the three states, respectively.

III. Computational Methods

The starting point of the numerical calculations is the potential matrix of eq 12, which enters the Hamiltonian of either the time-independent (TISE) or the time-dependent Schrödinger equation (TDSE). To solve the Schrödinger equation we use the multi-configuration time-dependent Hartree (MCTDH) method,[21,20,25−28] a mean field approach in which each degree of freedom is associated with a small number of orbitals or single-particle functions which, through their dependence on time, allow to efficiently describe the entire molecular dynamics process. The total wave function is expanded in Hartree products, that is, products of single-particle functions. The ansatz for the MCTDH wave function reads

$$\Psi(q_1, ..., q_f, t) \equiv \Psi(Q_1, ..., Q_p, t)$$
$$= \sum_{j_1}^{n_1} ... \sum_{j_p}^{n_p} A_{j_1, ..., j_p}(t) \prod_{\kappa=1}^{p} \varphi_{j_\kappa}^{(\kappa)}(Q_\kappa, t) \qquad (13)$$

where f denotes the number of degrees of freedom, and p is the number of MCTDH particles, also called combined modes. The particle coordinates Q_κ are logical coordinates that consist of one or several physical coordinates q_i. There are n_κ SPFs for the κth particle. The SPFs are finally represented by linear combinations of time-independent primitive basis functions. A discrete variable representation (DVR)[29,30] is used in practice. The MCTDH method hence propagates a wave function on a small time-dependent, variationally optimized basis set of single-particle functions, which in turn are defined on a time-independent grid with N_κ points for the κth particle. In the limit $n_\kappa \to N_\kappa$, MCTDH becomes a numerically exact method to solve the Schrödinger equation; however, convergence is usually obtained for rather small n_κ.

To represent the radial degrees of freedom, r_1 and r_2, we use a sine DVR with 70 grid points. The variables θ and k are combined and their dynamics is described by two-dimensional SPFs. These are represented by the so-called extended Legendre DVR, or KLeg, which is a two-dimensional DVR[31] in the mixed representation (θ, k). For details see the appendix of ref 32.

The MCTDH method is not only used to propagate wave-packets, but also to generate eigenvector/eigenvalue pairs. To this end the MCTDH ansatz, eq 13, is applied to a time-independent variational principle and the resulting equations are iteratively solved by a mixture of diagonalization and propaga-

tion in negative imaginary time. This so-called improved relaxation algorithm is described in refs 28, 33, and 34.

When computing photoelectron (PE) spectra, we adopt the Condon approximation and assume that the transition dipole operator is independent of the coordinates. The initial wave function in the time-dependent picture is hence the vibrational ground state wave function of the electronic neutral ground state potential placed vertically on one of the three (coupled) ionic surfaces of eq 12. This wavepacket is propagated and its autocorrelation function, $c(t) = \langle \Psi(0)|\Psi(t) \rangle$, is Fourier transformed to obtain the spectrum. To be precise, the expression to be evaluated is

$$\sigma(\omega) = \frac{1}{\pi} \int_0^T \text{Re}[c(t) \exp(i\omega t)] \cos^2(\pi t/2T) dt \quad (14)$$

where T is the propagation time. As the propagation time T is finite, the damping term $\cos^2(\pi t/2T)$ serves to remove artifacts due to the Gibbs phenomenon. It corresponds to a convolution of the exact spectrum with the filter function

$$\tilde{g}(\omega) = \frac{\pi^2 \sin(\omega T)}{\omega(\pi - \omega T)(\pi + \omega T)} \quad (15)$$

which has a fwhm of 4.1 eV fs. In our calculations, the propagation time is $T = 2000$ fs, yielding line widths of approximately 2 meV fwhm. The three spectra obtained from the three initial wave functions were summed with equal weights.

For a better understanding of the vibrational structure of the spectra, we compared them to the eigenstates of the Hamiltonian $\mathbf{T} + \mathbf{W}$, obtained for all values of K. Often several eigenstates are nearly degenerate close to a spectral line. Calculating the overlap of an eigenstate with the initial wave function of the propagation helps to decide which state contributes to the spectrum and which one is dark. After that, vibrational assignments of the eigenstates have been made with the help of reduced density plots in the (r_1, θ) or (r_1, r_2) plane. This leads to the mode numbering (ν_1, ν_2, ν_3) of the eigenstates, where ν_1 and ν_3 are the symmetric and antisymmetric stretching modes and ν_2 is the bending mode.

For $K > 0$, due to the Renner–Telling coupling, the eigenstates can often not be attributed clearly to one of the electronic states X or A. Writing the nuclear wave function χ of the Renner–Teller subspace after diabatization as

$$\chi = \begin{pmatrix} \chi_+ \\ \chi_- \end{pmatrix} = \mathbf{S}_2 \begin{pmatrix} \chi_X \\ \chi_A \end{pmatrix} = \frac{1}{\sqrt{2}} \begin{pmatrix} \chi_A + i\chi_X \\ \chi_A - i\chi_X \end{pmatrix} \quad (16)$$

we introduce the probabilities P_X and P_A

$$P_{X/A} = ||\chi_{X/A}||^2 \quad (17)$$

to find the nuclear wavepacket in the X or A states, respectively. These probabilities, and hence the degree of mixing, can be inferred calculating the expectation value of the matrix

$$\sigma_1 = \begin{pmatrix} 0 & 1 \\ 1 & 0 \end{pmatrix} \quad (18)$$

which yields

$$\langle \sigma_1 \rangle = ||\chi_A||^2 - ||\chi_X||^2 = P_A - P_X \quad (19)$$

From this follows

$$P_X = \frac{1}{2}(1 - \langle \sigma_1 \rangle) \quad (20)$$

$$P_A = \frac{1}{2}(1 + \langle \sigma_1 \rangle) \quad (21)$$

IV. Computational Results

Figure 1 shows two theoretical PE spectra and experimental results taken from ref 3 The calculated spectra were further convoluted with a Gaussian function to simulate a line width of about 11 meV fwhm as given in ref 3. The uppermost spectrum stems from a propagation on the adiabatic PES (X^2A'', A^2A', and B^2A') while the spectrum in the middle was calculated using the diabatic states as derived in Section II.

The agreement with the experiment is very good in the X-band (between 12 and 13.5 eV) for both the adiabatic and the diabatic approaches. Concerning the A and B bands (14–16.5 eV and 17–20.5 eV, respectively), the overall shape of the experimental spectra is well reproduced only by the diabatic calculation. The obvious difference to the experiment is the shift of the center of gravity of the A and B bands to higher binding energies in our results.

Concerning the adiabatic calculation, the main difference is the highly resolved vibrational structure in the B band, which we consider to be artificial, in the absence of vibronic coupling. Also, the line spacings in the A band seem to be twice as large as compared to the diabatic results and the experiment. This stems from the lack of vibronic states with even values of K. (In the adiabatic calculation, $k = 0$, corresponding to an odd value of the total angular momentum projection K.) Without Renner–Teller coupling we also do not observe line splittings.

In the following the three spectral bands will be investigated separately.

A. X^2B_1 State. Figure 2 displays the computed photoelectron spectrum in the energy region of the X-band together with experimental results from ref 3. Three individual spectra with $K = 0$, 1, and 2 (the lowest vibronic states Σ, Π, and Δ) have been calculated. Higher vibronic states have been excluded for this band upon comparison with the highly resolved, rotationally cold, experimental spectrum. To our knowledge, however, no vibronic splitting of the spectral lines in the X-band has been accounted for in experimental publications. After convolution with a Gaussian, the three theoretical spectra have been summed up with equal weight and shifted in energy to match the experimental value for the adiabatic ionization energy of the X-state, 12.621 eV.

The additional term proportional to k^2 in the kinetic energy, compare eq 7, gives rise to a shift of the vibronic energy levels and spectral lines as compared to an adiabatic calculation (where $k = 0$). Examining this shift $\Delta E_{(\nu_1, \nu_2, \nu_3)}$ for each vibrational mode (ν_1, ν_2, ν_3), the shift can be expressed as a mode-specific energy $\Delta E^0_{(\nu_1, \nu_2, \nu_3)}$ times the average of the squared values of k for any given value of K:

$$\Delta E_{(\nu_1, \nu_2, \nu_3)} = \Delta E^0_{(\nu_1, \nu_2, \nu_3)} \frac{(K-1)^2 + (K+1)^2}{2}$$
$$= \Delta E^0_{(\nu_1, \nu_2, \nu_3)}(K^2 + 1) \quad (22)$$

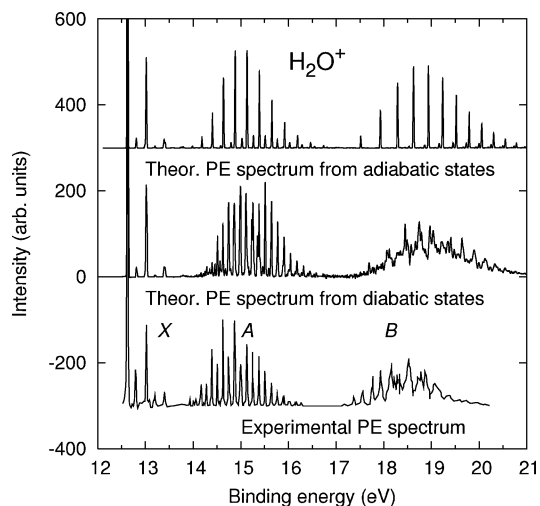Nonadiabatic Nuclear Dynamics of Ionized H₂O

J. Phys. Chem. A, Vol. 114, No. 36, 2010 **9897**

Figure 1. Photoelectron (PE) spectrum of H_2O^+. Calculated are the PE bands corresponding to the cationic X^2B_1, A^2A_1, and B^2B_2 states (12−13.5, 14−16.5, and 17−20.5 eV, respectively). The uppermost spectrum (shifted upward by 300 units) is obtained using the adiabatic states only, the middle spectrum from a diabatic calculation. Experimental results (lower spectrum, shifted downward by 300 units) taken from ref 3. All spectra are normalized to 1000 units at the first peak (12.6 eV); the ordinate is cut at 600 units, though.
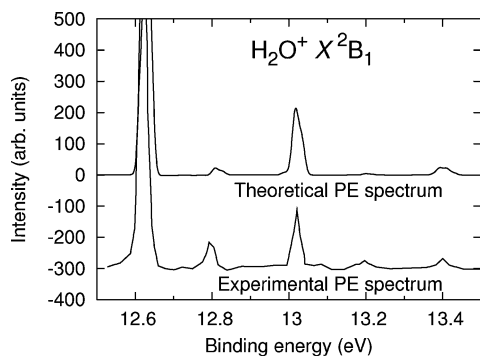

Figure 2. Expanded view of the photoelectron (PE) spectrum of H_2O^+ in the X band. Experimental results (shifted downward by 300 units) taken from ref 3.

The energy $\Delta E^0_{(\nu_1, \nu_2, \nu_3)}$ is proportional to $\langle \sin^{-2}\theta \rangle$. As the equilibrium angle of H_2O^+ in the X^2B_1 state is approximately 110°,[3] the $\sin^{-2}$ function increases for increasing angle, or higher values of ν_2, and $\Delta E^0_{(\nu_1, \nu_2, \nu_3)}$ should increase. On the other hand, if the expectation values of r_1 and r_2 increase (or for higher values of ν_1 and ν_2), $\Delta E^0_{(\nu_1, \nu_2, \nu_3)}$ is expected to decrease due to the $1/r^2$ dependence of the kinetic terms which include the $\hat{j}^2$ operator.

These expectations are confirmed by the data displayed in Table 1, where the energy shifts for all K values are recorded.

The energies used for Table 1 result from a calculation of the eigenstates of the Hamiltonian $\mathbf{T} + \mathbf{W}$. In addition to the lines visible in the spectrum (cf. Table 2), splittings are given for all vibrational eigenstates with quanta up to $2(\nu_1 + \nu_3) + \nu_2 = 5$

Table 2 lists the mode labels and related line intensities of the theoretical, nonconvoluted spectra compared to experimental values taken from refs 1 and 3. The comparison shows that relative intensities are in general in good agreement with the experiment, except for the (0,1,0) and (1,1,0) modes, which have considerably lower intensity in the calculations.

Finally, Table 3 lists the vibrational energies of the Σ, Π, and Δ vibronic states together with experimental values. The

(0,0,0) mode is chosen as the zero point of the energy. The vibrational spacings for the bending mode are slightly too high, whereas for the symmetric stretching mode the energies are lower than the experimental values. In ref 1 the following values are given: $h\nu_1 = (405 \pm 10)$ meV and $h\nu_2 = (178 \pm 10)$ meV. Thus, these experimental and the present theoretical values agree within the experimental error of ± 10 meV.

B. A^2A_1 State. An expanded view of the PE spectrum is shown in Figure 3 in the energy region of the A^2A_1 state. The experimental spectrum is again taken from ref 3. Calculations with all values of K from 0 to 5 have been convoluted with a Gaussian and summed up with equal weight. As was already stated above, the center of gravity of the calculated curve lies at higher energies compared to the experimental one: The most intense line in exp. (a) (ref 1) is the (0,7,0) Σ mode, and in exp. (b) (ref 3) it is the (0,8,0) Π mode. In our calculation, however, the (0,11,0) Σ mode is the most intense one.

The vibrational assignments are obtained following the procedure outlined in Section III. To confine the computational effort, only the eigenstates up to the (0, 11, 0) mode were evaluated. However, it is obvious that the most prominent spectral lines arise from the $(0, \nu_2, 0)$-progression. Table 4 lists vibrational energies of the A state with respect to the (0, 0, 0) ground state. The Renner−Teller effect leads to a splitting of the spectral lines, as was already observed in Section IV.1. For each mode with even value of ν_2, only odd values of K appear and vice versa because of momentum conservation.[3] Moreover, for the three lowest modes, transitions to higher values of K are forbidden.

We also give the Renner−Teller splitting for the $(1, \nu_2, 0)$-progression that was not resolved in the experiment. There, only the position of the centroid could be recorded.

The Renner−Teller effect causes the mixing of vibrational states pertaining to either the X or the A electronic states. For the strongest lines, belonging to the $(0, \nu_2, 0)$-progression, the percentage P_A mostly exceeds 70%. A study of the highly resolved, nonconvoluted spectra reveals that several lines are split into two components with a considerable percentage P_X, for example, into the (0, 7, 0) Δ and the (0, 12, 0) mode, which was attributed to the X state. Figure 4 displays the Σ spectrum (where there is no Renner−Teller effect and hence all lines belong exclusively to the A state) and the Δ spectrum. Most of the lines with low intensity in the latter spectrum stem from vibrational states of the X electronic state. Also, several lines of the $(0, \nu_2, 0)$ progression appear to be split, like the aforementioned (0, 7, 0) line and presumably also the (0, 13, 0) and (0, 17, 0) lines (at 14.5, 15.25, and 15.75 eV binding energy, respectively).

Apart from the splitting between X and A vibrational states, Figure 4 also shows the $\Sigma - \Delta$ splitting, which is stronger for lower binding energies. This applies also for the $\Pi - \Phi$ splitting. Averaging over the (0, 3, 0)−(0, 15, 0) modes for the $\Sigma - \Delta$ splitting and the (0, 4, 0)−(0, 16, 0) modes for the $\Pi - \Phi$ splitting, we obtained 14 and 17 meV, respectively. The first value is in very good agreement with the experimental results of 14 meV[1] and of 14.8 meV.[3] The $\Pi - \Phi$ splitting, however, was reported to be 23 and 28 meV by refs 1 and 3, respectively.

Comparing the vibrational energies of the (0, 0, 0) Π and (0, 1, 0) Σ modes, we found a value of 113 meV for the energy of the ν_2 quantum, which is similar to experimental results (112 meV in ref.[1]). For the ν_1 quantum, a value of 381 meV is found upon comparing the energies of the (0, 0, 0) Π and (1, 0, 0) Π modes (391 meV in ref 1).

9898 *J. Phys. Chem. A, Vol. 114, No. 36, 2010*

Eroms et al.

TABLE 1: Energy Shifts for Vibronic States Σ, Π, Δ, Φ, Γ, and G in the X^2B_1 State with Respect to the Adiabatic ($k = 0$) Case[a]

mode				energies (in meV)			
	Σ ($K = 0$)	Π ($K = 1$)	Δ ($K = 2$)	Φ ($K = 3$)	Γ ($K = 4$)	G ($K = 5$)	$\Delta E^0_{(\nu_1,\nu_2,\nu_3)}$
(0,0,0)	5	10	25	49	83	127	4.9
(0,1,0)	6	11	27	53	90	136	5.3
(0,2,0)	6	12	30	58	98	147	5.8
(1,0,0)	5	10	24	48	82	125	4.8
(0,0,1)	4	9	23	47	80	122	4.6
(0,3,0)	7	14	34	65	108	161	6.5
(1,1,0)	6	11	27	52	89	135	5.3
(0,1,1)	5	10	25	51	86	131	5
(0,4,0)	9	16	39	75	123	180	7.5
(1,2,0)	6	12	29	56	98	147	5.8
(0,2,1)	6	12	28	56	97	144	5.8
(2,0,0)	5	9	23	47	77	120	4.6
(0,0,2)	5	9	23	47	76	119	4.6
(1,0,1)	5	9	23	47	79	121	4.7
(0,5,0)	13	22	49	91	145	207	9
(1,3,0)	7	14	33	64	104	164	6.5
(0,3,1)	7	13	32	62	102	159	6.3
(2,1,0)	5	10	25	50	87	127	5
(0,1,2)	5	10	25	50	87	125	5
(1,1,1)	5	10	25	50	85	130	5

[a] Mode labelling (ν_1, ν_2, ν_3) refers to symmetric stretch, bending, and asymmetric stretch. Note that not all modes contribute to the spectrum, cf. Table 2. The energy shifts can to a high accuracy be expressed as $\Delta E_{(\nu_1,\nu_2,\nu_3)} = \Delta E^0_{(\nu_1,\nu_2,\nu_3)}(K^2 + 1)$.

TABLE 2: Line Intensities of the Σ, Π, and Δ Vibronic States in the X^2B_1 State Compared to Experimental Values[a]

mode	Σ	Π	Δ	exp.[b]	exp.[c]
(0,0,0)	1.000	1.000	1.000	1.000	1.000
(0,1,0)	0.030	0.024	0.021	0.127	0.089
(0,2,0)	0.010	0.009	0.010	0.037	0.010
(1,0,0)	0.209	0.213	0.218	0.201	0.193
(1,1,0)	0.005	0.004	0.004	0.041	0.016
(1,2,0)	0.003	0.003	0.004	0.050	0.003
(2,0,0)	0.020	0.018	0.018	0.085	0.023

[a] Intensities are normalized to the (0,0,0) mode. These modes are the most relevant ones for the spectrum. [b] Reference 1. [c] Reference 3.

TABLE 3: Vibrational Energies (in eV) of the Σ, Π, and Δ Vibronic States in the X^2B_1 State[a]

mode	Σ	Π	Δ	Exp.[b]	Exp.[c]	Exp.[d]	Exp.[e]
(0,1,0)	0.186	0.187	0.188	0.178	0.175	0.173	0.177
(0,2,0)	0.367	0.368	0.371	0.349	0.344	0.336	−
(1,0,0)	0.396	0.395	0.395	0.405	0.398	0.397	0.402
(1,1,0)	0.578	0.579	0.580	0.582	0.570	0.567	0.576
(1,2,0)	0.756	0.756	0.759	0.756	0.736	0.730	−
(2,0,0)	0.770	0.770	0.769	0.784	0.779	0.782	0.793

[a] The zero point of the energy is in the (0,0,0) mode. Spacings are slightly higher for the bending modes and lower for the stretching modes as compared to experimental values. [b] Reference 1. [c] Reference 3. [d] Reference 5. [e] Reference 6.

C. B^2B_2 State. The spectrum of the B^2B_2 state, which is displayed in Figure 5, exhibits a rather complex vibrational pattern. Its origin was ascribed to a strong excitation of the modes ν_1 and ν_2 in refs 1, 3, 6, and 7, whereas ref 5 suggested excitations of the stretching modes ν_1 and ν_3, instead.

For the system with three coupled states, wavepacket propagations and the evaluation of the spectrum according to eq 14 are computationally much less challenging than a calculation of the vibrational eigenstates. As the vibrational eigenstates of the B^2B_2 state are embedded in the manifold of states pertaining to the Renner−Teller subsystem, higher
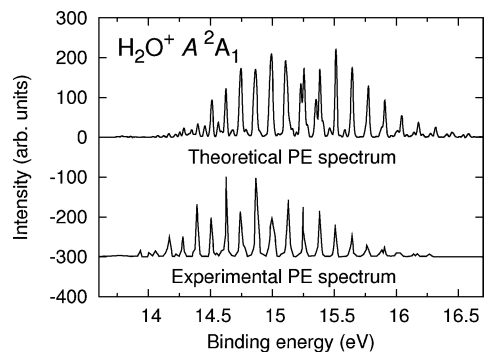
Figure 3. Expanded view of the photoelectron (PE) spectrum of H_2O^+ in the A band. Experimental results (shifted downward by 300 units) taken from ref 3.

eigenstates than the (0, 0, 0)-mode could only be obtained diagonalizing the A, B-subsystem or, neglecting the conical intersection, using only the diabatic W_{22} PES. There, the highest overlaps were found for eigenstates with combined excitations of the ν_1 and ν_2 modes, affirming the experimental results mentioned above.

For the vibrational quantum ν_1, the energy $h\nu_1 = 293$ meV was found, which differs considerably from the experimental value $h\nu_1 = 360$ meV.[1] The theoretical result for the quantum ν_3 is $h\nu_3 = 212$ meV (experimental value: $h\nu_3 = 352$ meV[1]). For the bending mode quantum, theory and experiment agree better. We found $h\nu_2 = 171$ meV, which is 10% less than the experimental result $h\nu_2 = 190$ meV.[1]

In the experiment, it is difficult to assign the correct value for the adiabatic ionization potential (AIP) of the B^2B_2 state, given the low intensities at the onset of the B-band. Experimental results so far are 17.203 eV,[1] 17.183 eV,[5] 17.189 eV,[6] and 17.22 eV.[7] From our calculations, however, a lower AIP seems more appropriate. For $k = 0$, which gives the lowest energy, we find a value of 16.76 eV. As was explained in ref 8, the absolute energetic positions of the PESs can be off by a fraction of an eV, which might explain the energy shift.

Finally, the equilibrium geometry of the B^2B_2 state, was found from density plots of the (0, 0, 0) mode, to be $R_{OH} = 2.24$ a_0, θ

TABLE 4: Energies (in eV) and Relative Intensities of the Most Intense Vibrational Modes of the A PE Band[a]

mode	K	Theory			Exp.[b]		Exp.[c]	
		Energy	Intensity	P_A	Energy	Intensity	Energy	Intensity
(0,0,0)	Π	0.000	0	19.1	0.000	427	—	—
[0,1,0]	Δ	0.058	0	11.5	—	—	—	—
(0,1,0)	Σ	0.113	8	100.0	0.087	314	0.094	11
[0,2,0]	Φ	0.124	0	7.6	—	—	—	—
(0,2,0)	Π	0.186	11	78.7	0.199	377	0.191	69
[0,3,0]	Γ	0.196	0	5.2	0.280	284	—	—
(0,3,0)	Δ	0.262	21	73.9	0.295	337	0.298	25
(0,3,0)	Σ	0.300	36	100.0	0.310	389	0.303	51
[0,4,0]	G	0.271	1	2.4	0.370	463	—	—
(0,4,0)	Φ	0.348	37	78.2	0.384	449	0.393	71
(0,4,0)	Π	0.390	74	78.9	—	—	0.416	244
(1,0,0)	Π	0.381	1	16.5	0.321	462	0.315	25
(0,5,0)	Γ	0.445	50	84.8	0.479	385	0.476	31
(0,5,0)	Δ	0.479	101	69.8	0.512	478	0.516	113
(0,5,0)	Σ	0.510	137	100.0	0.527	637	0.526	222
[1,1,0]	Δ	0.434	0	9.9	—	—	—	—
(1,1,0)	Σ	0.513	56	100.0	0.420	590	0.425	20
[1,2,0]	Φ	0.496	0	7.0	—	—	—	—
(1,2,0)	Π	0.578	7	72.4	0.539	780	0.538	22
(0,6,0)	G	0.553	69	89.7	0.608	419	—	—
(0,6,0)	Φ	0.574	157	55.3	0.623	499	0.617	68
(0,6,0)	Π	0.622	250	66.0	0.650	725	0.643	671
(1,6,1)X	Π	0.630	36	11.5	—	—	—	—
(1,3,0)	Δ	0.652	5	74.6	—		—	
(1,3,0)	Σ	0.696	7	100.0	0.671	709	0.655	33
(0,7,0)	Γ	0.679	196	70.5	0.712	460	0.700	25
(0,7,0)	Δ	0.726	189	46.7	0.745	544	0.755	406
(0,12,0)X	Δ	0.739	194	46.0	—	—	—	—
(0,7,0)	Σ	0.738	537	100.0	0.763	1000	0.763	216
(1,4,0)	Φ	0.738	5	80.4	—	—	—	—
(1,4,0)	Π	0.787	1	44.7	0.776	911	0.774	42
(0,8,0)	G	0.789	192	53.8	0.824	498	0.805	56
(3,4,0)X	G	0.797	27	9.0	—	—	—	—
(2,7,0)X	Φ	0.845	165	18.6	—	—	—	—
(0,8,0)	Φ	0.847	251	46.0	0.855	510	0.854	78
(0,8,0)	Π	0.853	662	90.3	0.871	628	0.892	1000
(1,5,0)	Γ	0.835	8	84.3	—	—	—	—
(1,5,0)	Δ	0.857	18	42.2	—	—	—	—
(1,5,0)	Σ	0.904	19	100.0	0.888	888	0.904	36
(0,9,0)	Γ	0.958	427	57.5	0.944	482	—	—
(0,9,0)	Δ	0.968	773	84.1	0.965	479	0.994	474
(0,9,0)	Σ	0.977	874	100.0	0.979	515	1.006	387
(1,6,0)	G	0.941	6	75.2	—	—	—	—
(1,6,0)	Φ	0.950	19	46.4	—	—	—	—
(1,6,0)	Π	1.011	33	77.1	1.007	768	1.029	121
(0,10,0)	G	1.074	614	67.1	1.078	455	—	—
(0,10,0)	Φ	1.085	816	78.8	1.100	430	1.099	77
(0,10,0)	Π	1.097	944	—	1.119	514	1.127	986
(1,7,0)	Γ	1.049	16	38.2	—	—	—	—
(1,7,0)	Δ	1.078	29	15.6	—	—	—	—
(1,7,0)	Σ	1.129	63	100.0	1.140	687	1.143	134
(0,11,0)	Γ	1.203	832	—	1.203	352	—	—
(0,11,0)	Δ	1.215	955	—	1.238	387	1.238	286
(0,11,0)	Σ	1.225	1000	—	1.253	496	1.253	426

[a] All vibronic symmetries $K = \Sigma, \Pi, \Delta, \Phi, \Gamma$, G are listed. Note that for the $(1, \nu_2, 0)$-modes, experimental results refer to the centroid of the line and not to a specific K value. Energies are relative to the (0,0,0)-mode and the intensity of the most prominent lines in theory and the two experiments is set to 1000. The Renner−Teller mixing of the X and A states is characterised by the probability P_A (in %), given by eq 20. A dash indicates where no experimental data is available or no eigenstates could be computed. Mode assignments are in square brackets if they are ambiguous. Vibrational modes of the X-state are labeled accordingly as some lines appear to be split into several components, cf. Figure 4. [b] Reference 1. [c] Reference 3.

$= 0.90$ rad ($= 51.6°$). This is in fair agreement with the previous estimation, given in ref 3, $R_{OH} = 2.16\ a_0$, $\theta = 0.96$ rad ($= 55.0°$).

V. Conclusion

In this article, the valence ionization of water molecules has been considered. The cationic states X^2B_1, A^2A_1, and B^2B_2 are subject to vibronic coupling prohibiting an adiabatic treatment of the dynamics. Instead, we have demonstrated how to perform a diabatization of the PESs in two steps to treat both the Renner−Teller coupling of the X^2B_1 and A^2A_1 states and the conical intersection between the A^2A_1 and B^2B_2 states. As a result, the kinetic energy operator is diagonal; the potential
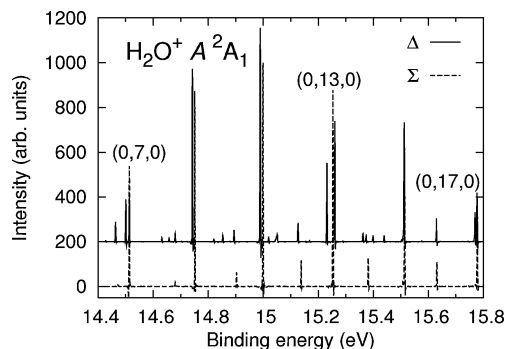
Figure 4. Spectra of the Σ and Δ symmetries in the A band of H_2O^+. In the lower spectrum, the Renner–Teller effect is absent as $K = 0$ (Σ). The upper spectrum ($K = 1$, Δ) reflects the Renner–Teller effect: Shift of the most intense lines to lower energies as compared to the Σ lines and splitting of several Δ lines into two components with a high percentage P_X each (the (0, 7, 0), (0, 13, 0) and (0, 17, 0) lines at 14.5, 15.25, and 15.75 eV).
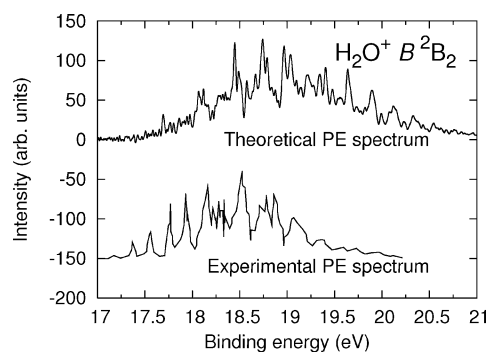

Figure 5. Expanded view of the photoelectron (PE) spectrum of H_2O^+ in the B band. Experimental results (shifted downward by 150 units) taken from ref 3.

energy matrix, however, contains off-diagonal elements that couple the three diabatic PESs.

The spectrum that consists of three distinct bands was computed performing a wave packet propagation and subsequent Fourier transformation of the autocorrelation function. Both the experimental and theoretical spectra are vibrationally resolved. To examine the vibrational excitation of the molecule, vibrational eigenstates and energies were obtained and compared to the spectral lines. For each band, we have shown which modes make the strongest contribution to the spectral intensity.

In the X^2B_1 state, only few excitations are relevant, as the geometry change upon ionization is rather small.

The A^2A_1 state is nearly linear and is strongly Renner–Teller coupled to the X state. Apart from the Renner–Teller splitting of the bending modes, which involves different values of the parameter K describing angular momentum, we have shown that there is also a splitting of lines with the same value of K. Here, the spectral intensity is distributed on nearly degenerate modes, which we have assigned to the bending progression of the A state and highly excited eigenstates with a strong X component.

The spectrum of the B^2B_2 state, which is the highest in energy is rather complex. It arises from vibrational states with excitations of both the symmetric stretching and the bending modes as was already pointed out in many experimental studies. Our value for the adiabatic ionization potential (AIP) of 16.76 eV is considerably lower than previous experimental results (approximately 17.2 eV). On the one hand, it is difficult to assign the AIP by inspection of the experimental spectra only, on the other hand, absolute energies of the PESs might vary by a

fraction of an electronvolt. For other spectroscopic parameters, like the mode quanta, the agreement with the experiment was in general very good among the three spectral bands as relative energies of the PESs are much more reliable.

Only for the X state, a calculation with the adiabatic PESs leads to good results, for the A and B state, the agreement is very poor. Therefore, the effort of diabatizing the PESs and performing calculations on coupled states has proven to be necessary for simulating the valence ionization of H_2O.

Appendix A: Derivation of the Diabatic Potential Energy Matrix for the Conically Intersecting States

For now, the X state is left aside. It will enter only through the Renner–Teller coupling, which will be considered later. The adiabatic potential energy matrix $\mathbf{V}$ of the full system reduces to the two-state subsystem $\mathbf{V}_{A,B}$, that is,

$$\mathbf{V}_{A,B} = \begin{pmatrix} V_A & 0 \\ 0 & V_B \end{pmatrix} \tag{A1}$$

An adiabatic-to-diabatic transformation $\mathbf{S}_1$ serves to diagonalize the kinetic energy part of the Hamiltonian matrix.

As a result of the diabatization of the A and B states, the potential energy matrix $\mathbf{V}_{A,B}$ will assume the following form

$$\mathbf{W}_{A,B} = \mathbf{S}_1 \mathbf{V}_{A,B} \mathbf{S}_1^\dagger = \begin{pmatrix} W_{11} & W_{12} \\ W_{12} & W_{22} \end{pmatrix} \tag{A2}$$

where $\mathbf{W}_{A,B}$ is a real symmetric matrix. The adiabatic potentials V_A and V_B are the eigenvalues of $\mathbf{W}_{A,B}$, hence:

$$V_{B/A} = \frac{1}{2}(W_{11} + W_{22}) \pm \frac{1}{2}\sqrt{(W_{11} - W_{22})^2 + 4W_{12}^2} \tag{A3}$$

Define

$$\Delta V = V_B - V_A, \quad \Delta W = W_{22} - W_{11},$$
$$\Sigma = \frac{1}{2}(V_A + V_B) \tag{A4}$$

then follows

$$\Delta V^2 = \Delta W^2 + 4W_{12}^2 \tag{A5}$$

$$\Sigma = \frac{1}{2}(W_{11} + W_{22}) \tag{A6}$$

The matrices $\mathbf{W}_{A,B}$ and $\mathbf{V}_{A,B}$ may hence be written

$$\mathbf{W}_{A,B} = \Sigma \cdot \mathbf{1} + \begin{pmatrix} -\dfrac{\Delta W}{2} & W_{12} \\ W_{12} & +\dfrac{\Delta W}{2} \end{pmatrix} \tag{A7}$$

$$\mathbf{V}_{A,B} = \Sigma \cdot \mathbf{1} + \begin{pmatrix} -\dfrac{\Delta V}{2} & 0 \\ 0 & +\dfrac{\Delta V}{2} \end{pmatrix} \quad \text{(A8)}$$

Due to symmetry considerations, the coupling mode is the nontotally symmetric mode.[15] Let Q_u denote the coupling mode and Q collectively all the other (totally symmetric) modes. For convenience, we define

$$\Delta V_0(Q) = \Delta V(Q, Q_u = 0) \quad \text{(A9)}$$

To obtain the diabatic surfaces from the adiabatic ones, two assumptions are made:
(i)

$$W_{12}(Q, Q_u) = Q_u \cdot K(Q, Q_u) \text{ with } K(Q, Q_u) \geq 0 \quad \text{(A10)}$$

In particular we have $W_{12}(Q, Q_u = 0) = 0$.
(ii) ΔW does not depend on Q_u, that is:

$$\Delta W(Q, Q_u) = \Delta W(Q, Q_u = 0) \quad \text{(A11)}$$

From these assumptions follows from eq A5

$$\Delta W^2 = \Delta V_0^2 \quad \text{(A12)}$$

$$4W_{12}^2 = \Delta V^2 - \Delta V_0^2 \quad \text{(A13)}$$

Hence

$$\Delta W = \pm \Delta V_0 \quad \text{(A14)}$$

$$W_{12} = Q_u \sqrt{\frac{\Delta V^2 - \Delta V_0^2}{4Q_u^2}} \quad \text{(A15)}$$

At this stage, $\mathbf{W}_{A,B}$ is given by

$$\mathbf{W}_{A,B} = \Sigma \cdot \mathbf{1} + \begin{pmatrix} \pm \dfrac{\Delta V_0}{2} & Q_u \sqrt{\dfrac{\Delta V^2 - \Delta V_0^2}{4Q_u^2}} \\ Q_u \sqrt{\dfrac{\Delta V^2 - \Delta V_0^2}{4Q_u^2}} & \mp \dfrac{\Delta V_0}{2} \end{pmatrix} \quad \text{(A16)}$$

The remaining ambiguity is now the sign of ΔV_0 in eq A16. While the adiabatic PESs are energetically ordered and avoid each other, now care has to be taken that the resulting diabatic surfaces do intersect at the geometry of the conical intersection. Requesting the continuity of the first derivative of ΔV_0 and a thorough inspection of cuts through the PESs is one possibility to determine the sign. In the present case, however, the ab initio

calculations of the adiabatic PESs also contained information about the symmetry of the wave function in C_{2v} symmetry. With this knowledge, it is possible to decide whether the plus or minus sign has to be chosen for W_{11} (and vice versa for W_{22}).

Our central assumption $\Delta W(Q, Q_u) = \Delta W(Q, Q_u = 0)$ usually holds to sufficient accuracy for small $|Q_u|$. The singularity in the kinetic coupling due to the conical intersection is hence removed by our transformation. For large $|Q_u|$, however, a violation of our assumption may lead to $\Delta V^2(Q, Q_u) < \Delta V_0^2(Q)$ and hence to an imaginary coupling element in eq A16. In such a case we set the coupling element to zero and replace ΔV_0 by ΔV. As we are far from the conical intersection, this replacement is inessential.

References and Notes

(1) Truong, S. Y.; et al. *Chem. Phys.* **2009**, *355*, 183.
(2) Page, R. H.; Larkin, R. J.; Shen, Y. R.; Lee, Y. T. *J. Chem. Phys.* **1988**, *88*, 2249.
(3) Reutt, J. E.; Wang, L. S.; Lee, Y. T.; Shirley, D. A. *J. Chem. Phys.* **1986**, *85*, 6928.
(4) Banna, M. S.; McQuaide, B. H.; Malutzki, R.; Schmidt, V. *J. Chem. Phys.* **1986**, *84*, 4739.
(5) Dixon, R. N.; Duxbury, G.; Rabalais, J. W.; Åsbrink, L. *Mol. Phys.* **1976**, *31*, 423.
(6) Karlsson, L.; et al. *J. Chem. Phys.* **1975**, *62*, 4745.
(7) Brundle, C. R.; Turner, D. W. *Proc. Roy. Soc. A* **1968**, *307*, 27.
(8) Eroms, M.; Vendrell, O.; Jungen, M.; Meyer, H.-D. *J. Chem. Phys.* **2009**, *130*, 154307.
(9) Schneider, F.; Di Giacomo, F.; Gianturco, F. A. *J. Chem. Phys.* **1996**, *105*, 7560.
(10) Brommer, M.; et al. *J. Chem. Phys.* **1993**, *98*, 5222.
(11) Weis, B.; Carter, S.; Rosmus, P.; Werner, H.-J.; Knowles, P. J. *J. Chem. Phys.* **1989**, *91*, 2818.
(12) Dehareng, D.; Chapuisat, X.; Lorquet, J.-C.; Galloy, C.; Raseev, G. *J. Chem. Phys.* **1983**, *78*, 1246.
(13) Jackels, C. F. *J. Chem. Phys.* **1980**, *72*, 4873.
(14) Thiel, A.; Köppel, H. *J. Chem. Phys.* **1999**, *110*, 9371.
(15) Köppel, H.; Gronki, J.; Mahapatra, S. *J. Chem. Phys.* **2001**, *115*, 2377.
(16) Köppel, H.; Schubert, B. *Mol. Phys.* **2006**, *104*, 1069.
(17) McCurdy, C. W.; Isaacs, W. A.; Meyer, H.-D.; Rescigno, T. N. *Phys. Rev. A* **2003**, *67*, 042708.
(18) Haxton, D. J.; Rescigno, T. N.; McCurdy, C. W. *Phys. Rev. A* **2007**, *75*, 012711.
(19) Gómez-Carrasco, S.; Köppel, H. *Chem. Phys.* **2008**, *346*, 81.
(20) Meyer, H.-D. Gatti, F. Worth, G. A. Eds. *Multidimensional Quantum Dynamics: MCTDH Theory and Applications*; Wiley-VCH: Weinheim, 2009.
(21) Beck, M. H.; Jäckle, A.; Worth, G. A.; Meyer, H.-D. *Phys. Rep* **2000**, *324*, 1.
(22) Gatti, F.; Iung, C.; Chapuisat, X. *J. Mol. Struct. (Theochem)* **1998**, *424*, 201.
(23) Gatti, F.; Iung, C. *Phys. Rep.* **2009**, *484*, 1.
(24) Loettgers, A.; et al. *J. Chem. Phys.* **1997**, *106*, 3186.
(25) Meyer, H.-D.; Manthe, U.; Cederbaum, L. S. *Chem. Phys. Lett.* **1990**, *165*, 73.
(26) Manthe, U.; Meyer, H.-D.; Cederbaum, L. S. *J. Chem. Phys.* **1992**, *97*, 3199.
(27) Meyer, H.-D. Multiconfiguration Time-Dependent Hartree Method. In *The Encyclopedia of Computational Chemistry*; Schleyer, P. v. R., Eds.; John Wiley and Sons: Chichester, 1998; Vol *5*, pp 3011−3018.
(28) Meyer, H.-D.; Worth, G. A. *Theor. Chem. Acc.* **2003**, *109*, 251.
(29) Light, J. C. Discrete Variable Representations in Quantum Dynamics. In *Time-Dependent Quantum Molecular Dynamics*; Broeckhove, J. Lathouwers, L., Eds.; Plenum: New York, 1992; pp 185−199.
(30) Light, J. C.; Carrington Jr, T. *Adv. Chem. Phys.* **2000**, *114*, 263.
(31) Corey, G. C.; Lemoine, D. *J. Chem. Phys.* **1992**, *97*, 4115.
(32) Sukiasyan, S.; Meyer, H.-D. *J. Phys. Chem. A* **2001**, *105*, 2604.
(33) Meyer, H.-D.; Le Quéré, F.; Léonard, C.; Gatti, F. *Chem. Phys.* **2006**, *329*, 179.
(34) Joubert Doriol, L.; Gatti, F.; Iung, C.; Meyer, H.-D. *J. Chem. Phys.* **2008**, *129*, 224109.